JOURNAL OF SPACECRAFT AND ROCKETS
Vol. 29, No. 2, March-April 1992

Navier-Stokes Flow Simulation of the Space Shuttle Main Engine Hot Gas Manifold

R.-J. Yang* and J. L. C. Chang†
Rockwell International, Canoga Park, California 91303
and
D. Kwak‡
NASA Ames Research Center, Moffett Field, California 94035

Incompressible viscous flow inside the turnaround duct, the fuel bowl, the transfer duct, and the racetrack of the Space Shuttle main engine hot gas manifold has been computed using the method of pseudocompressibility together with an implicit, approximate-factorization algorithm. A multiple-zone method is used to make solution of flows in complex geometries easy. A model that estimates the pressure loading for the shield and the injector post arrangement without solving the complex flowfield in the main injector region is proposed. The computed results show good qualitative agreement with experimental data.

Nomenclature

Cp	= static pressure coefficient
Cp_o	= mass-weighted total pressure coefficient
l	= mixing length
M	= total mass flow rate
P_o	= mass-weighted total pressure, $(1/M)\int[p + \frac{1}{2}(u^2+v^2+w^2)]\,dm$
QTE	= inlet (at turbine exit) flow dynamic head
ΔP	= difference in static pressure
κ	= von Kármán constant, 0.4
ξ_i	= generalized coordinates

Introduction

THE complex nature of flows encountered in modern propulsion systems makes analytical solutions to the Navier-Stokes equations impossible. Numerical solutions of the full equations become an alternative to understanding flowfields and provide insight necessary for components optimum design. For three-dimensional internal viscous flow simulation, a large number of grid points and, thus, a large size of computer storage is required. With the rapid evolution in supercomputers and solution methodologies, it is now feasible to simulate complex internal flows in arbitrary geometries by solving the full Navier-Stokes equations.

An efficient implicit finite difference algorithm based on Beam-Warming's approximate-factorization[1] method or Briley-McDonald's ADI method[2] has been developed for compressible flows. Extensions of the scheme coupled with the method of pseudocompressibility first proposed by Chorin[3] to incompressible viscous flows have been studied by Steger and Kutler,[4] Chang and Kwak,[5] and Kwak et al.[6] A computer code, INS3D, using primitive variables, which is suitable for three-dimensional incompressible viscous flow simulations in generalized curvilinear coordinates, was developed by Kwak et al.[6] Applications of the code to the flow simulations for the hot gas manifold (HGM) of the Space Shuttle main engine (SSME) has been successfully made by Chang et al.[7-9]

Figure 1 illustrates the arrangement for the SSME powerhead components. Figure 2 demonstrates the cross-sectional views of the computational grids for the newly proposed SSME HGM. With the origin located at the center of the main injector, the left-hand side is called the fuel side and the right-hand side is the oxidizer side. Inside the HGM, the fuel side hot gas discharged from the turbine enters the annular turnaround duct (TAD) and experiences a 180-deg turn before it diffuses into the fuel bowl. Then it flows into the racetrack of the main injector through three circular transfer ducts. There are hundreds of liquid oxygen (LOX) posts in the main injector region. The outer row of the posts are shielded, as shown in Fig. 3. Because of high gas temperature, the Mach number is less than 0.12. The flow is turbulent and is practically incompressible. Solutions for the fuel side with a configuration including TAD, bowl, and transfer duct had been obtained by Chang et al.[7,8] It is instructive to include the racetrack in the flow simulation for better understanding of the flow phenomena inside the HGM.

The present work presents the further development of the INS3D code and its application to the flow simulation of the HGM, including racetrack. To make the solution of flows in complex geometries easy, a method of multiple computational zones is further advanced. A simple model that estimates the pressure loading for the shield and post arrangement without solving the complex flowfield inside the main injector region is proposed. Comparisons of the numerical solutions with the experimental data are presented. The current flow simulation represents an example of how the CFD can be applied to the real-world problems and illustrates its capability to pinpoint the area where design improvement is necessary.

Description of the Method

The present flow simulation uses INS3D as a base code. The formulation and the algorithm used in developing the code are discussed in detail by Kwak et al.[6] The key features of the methodologies adopted in the present study are outlined in the following.

Method of Pseudocompressibility

To achieve an efficient computation in solving steady-state incompressible flows, Chorin[3] proposed the use of artificial

Presented as Paper 87-0368 at the AIAA 25th Aerospace Sciences Meeting, Reno, NV, Jan. 12-15, 1987; received May 25, 1991; revision received Nov. 5, 1991; accepted for publication Nov. 6, 1991.

*Senior Member of Technical Staff, Rocketdyne Division. Member AIAA.
†Senior Staff Scientist, Rocketdyne Division. Member AIAA.
‡Research Scientist. Associate Fellow AIAA.

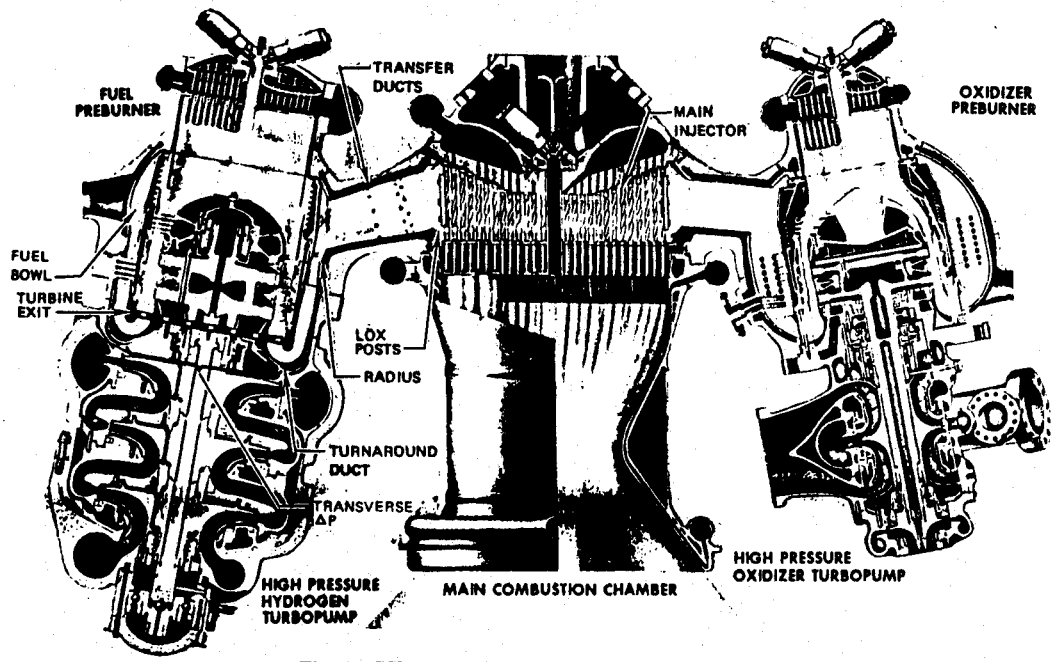

Fig. 1 SSME powerhead component arrangement.

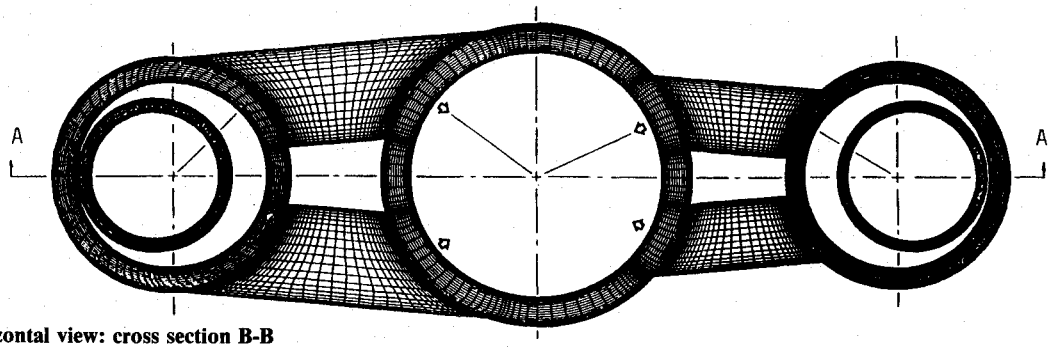

a) Horizontal view: cross section B-B

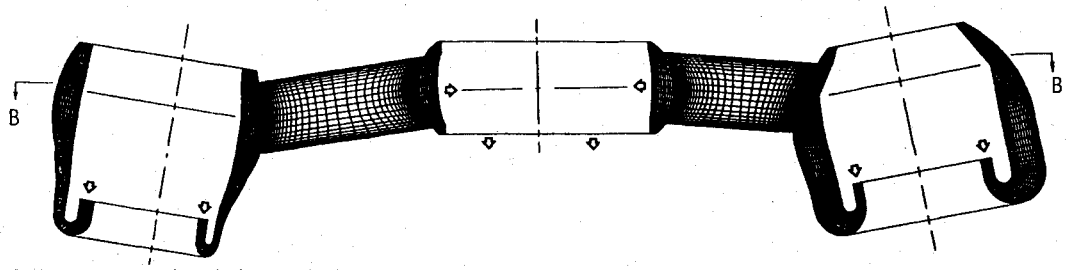

b) Vertical view: cross section A-A

Fig. 2 Grid for the SSME powerhead.

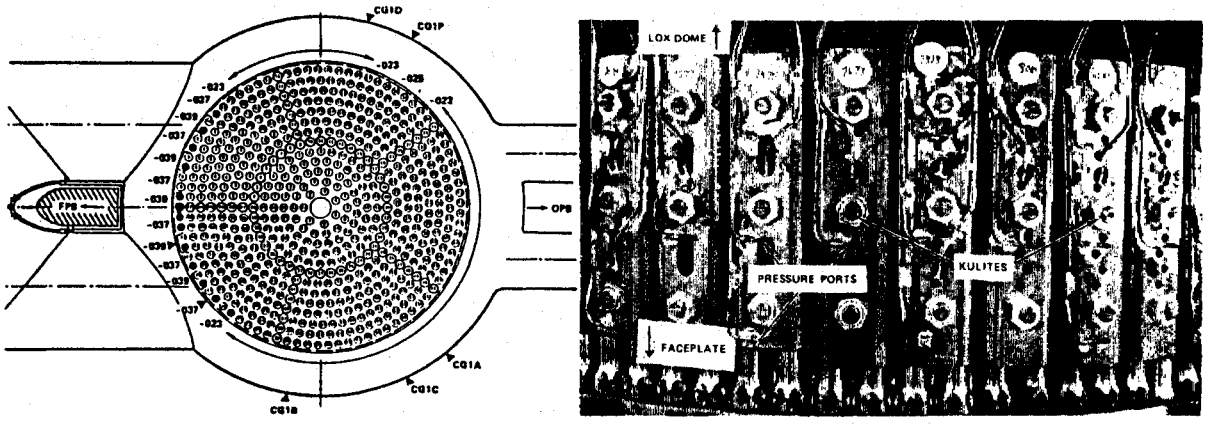

Fig. 3 Shield and post arrangement.

compressibility. This method was later studied by Steger and Kutler.[4] It was further developed into a method of pseudocompressibility by Chang and Kwak[5] and Kwak et al.[6] By this method, the incompressible Navier-Stokes equations in dimensionless form are modified as follows:

$$\frac{1}{\beta}\frac{\partial p}{\partial t} + \frac{\partial u_i}{\partial x_i} = 0$$
$$\frac{\partial u_i}{\partial t} + \frac{\partial u_i u_j}{\partial x_j} = -\frac{\partial p}{\partial x_i} + \frac{\partial \tau_{ij}}{\partial x_j} \tag{1}$$

where $1/\beta$ is the pseudocompressibility parameter, p the pressure, u_i the velocity components, τ_{ij} the stress tensors, t the time, and the indices i,j refer to the space coordinates x, y, and z. As the computation converges to a steady state, the effect of pseudocompressibility vanishes, yielding an incompressible solution.

Numerical Algorithm

To accommodate arbitrary three-dimensional geometries, the coordinates are transformed by using the following independent variables:

$$\tau = t$$
$$\xi_i = \xi_i(x,y,z,t) \tag{2}$$

In these generalized curvilinear coordinates, the governing equations in conservation-law form are expressed as

$$\frac{\partial \hat{Q}}{\partial \tau} + \frac{\partial(\hat{E}_i - \hat{\Gamma}_i)}{\partial \xi_i} = 0 \tag{3a}$$

The pressure and velocity vector $\hat{Q}$, the flux vector $\hat{E}$, and the viscous diffusion vector $\hat{\Gamma}$ are described by

$$\hat{Q} = \frac{Q}{J} = \frac{1}{J}\begin{bmatrix} p \\ u \\ v \\ w \end{bmatrix}, \quad \hat{E}_i = \frac{1}{J}\begin{bmatrix} \beta U_i + L_{i0}(p-\beta) \\ uU_i + L_{i1}p \\ vU_i + L_{i2}p \\ wU_i + L_{i3}p \end{bmatrix} \tag{3b}$$

$$\hat{\Gamma}_i = \frac{\nu}{J}(\nabla\xi_i \cdot \nabla\xi_j)\frac{\partial}{\partial \xi_j}[0,u,v,w]^T + \text{Reynolds stress terms}$$

where J is the Jacobian of the transformation, and

$$U_i = L_{i0} + L_{i1}u + L_{i2}v + L_{i3}w$$
$$L_{i0} = (\xi_i)_t, \qquad L_{i1} = (\xi_i)_x \tag{3c}$$
$$L_{i2} = (\xi_i)_y, \qquad L_{i3} = (\xi_i)_z$$

are the contravariant velocities and the metrics of transformation, respectively.

An implicit finite differnce algorithm together with an ADI or approximate-factorization scheme[1,2] are used to advance solution to Eq. (3a) in time. These procedures have been implemented to develop a three-dimensional incompressible Navier-Stokes flow solver (INS3D).[6]

Geometry and Grid

The configuration considered in the present study includes the fuel side TAD, the bowl, the elliptical transfer duct, and 70% racetrack of the main injector as shown in Figs. 4. In the flow environment, 70% of the total mass flow is delivered through the fuel side transfer ducts and the other 30% from the oxidizer side. Notice that flow enters the main injector through the small gaps between the shield and the small hole in the shield (see Fig. 3). The effective flow area per unit length is much smaller than the radial cross-sectional area of the racetrack. Therefore, a uniform radial outflow may be used to approximate the flow entering into the main injector region. Based on this argument, it can be said that 70% of the main injector flow area receives approximately 70% of the total mass flow. This argument has been qualitatively confirmed by an airflow test.[10] Hence, only 70% racetrack of the main injector is used in the present formulation. Figure 4a shows the

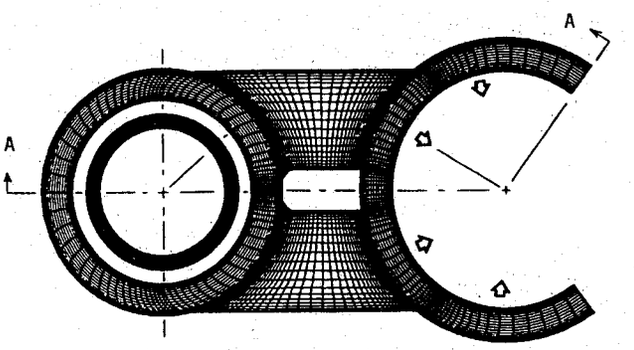

Fig. 4a Horizontal view: cross-section B-B.

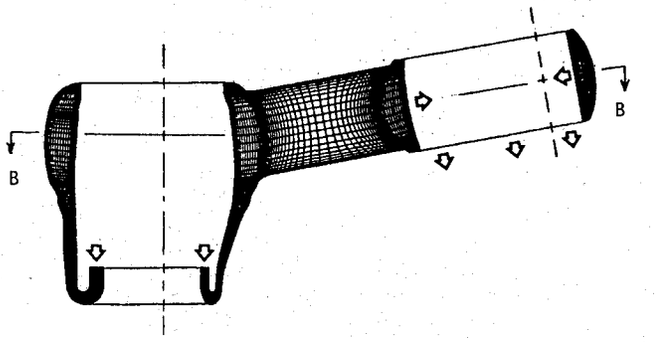

Fig. 4b Vertical view: cross section A-A.

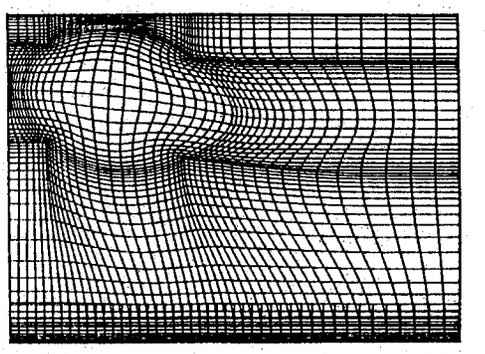

Fig. 5a Unwrapped surface grid of annular fuel bowl.

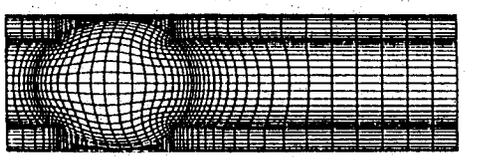

Fig. 5b Unwrapped surface grid of 70% racetrack.

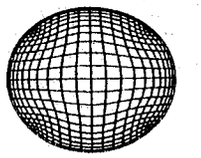

Fig. 5c Cross-sectional grid of transfer duct.

horizontal cross-sectional view of the HGM, whereas Fig. 4b gives a vertical view at the surface of the cross section. Figures 5a and 5b illustrate the unwrapped surface grids of the annular fuel bowl and the racetrack, respectively, and Fig. 5c shows the cross-sectional grid of the elliptical transfer duct. The grid for the entire HGM system is generated by using algebraic functions. Dense grids are placed in the regions where rapid flow changes are anticipated. Smoothness of the grid variation is controlled by a power factor determined by the wall and the core grid sizes and the assigned number of mesh points. The number of mesh points in each zone are as follows: $103\times52\times21$ for the fuel bowl, $23\times23\times45$ for the transfer duct, and $41\times53\times21$ for the racetrack, respectively. The total mesh points are 181,914. The minimum cell size in each zone is 0.001 in.

Multiple-Zone Method

For geometrically complicated problems such as the current HGM, a large number of grid points is required to resolve the three-dimensional viscous flow. The restriction in the computer in-core memory is still one of the main factors in today's Navier-Stokes code development for solutions of many realistic geometries. To make the solution of flows in complex geometries easy and to take advantage of the input-output solid-state devices (SSD) of the CRAY-XMP computer, a zonal method was developed by Chang et al.[7-9] The method is extended in the current work. By this method, the domain of interest is divided into several zones, as shown in Fig. 6; a special treatment at the interface is necessary for smooth continuations of the solution between zones of abrupt change in geometry. Note that in Fig. 6 the overlap regions are extended from zone 2 into zone 1 and zone 3, respectively. This method avoids extra computer storage and also makes the ADI sweep simple.

Turbulence Model

The model used in the present paper is an extended Prandtl-Kármán mixing length theory.[8] The length scale is based on the vorticity thickness δ_ω, defined as the distance between the wall and the location of minimum vorticity. The expression is given as

$$\frac{l}{\delta_\omega} = \kappa^2(1-e^{-\tilde{y}/\kappa}), \qquad \tilde{y} = \frac{y}{\delta_\omega} \tag{4}$$

and the eddy viscosity is given by

$$\nu_t = l^2|\omega| \tag{5}$$

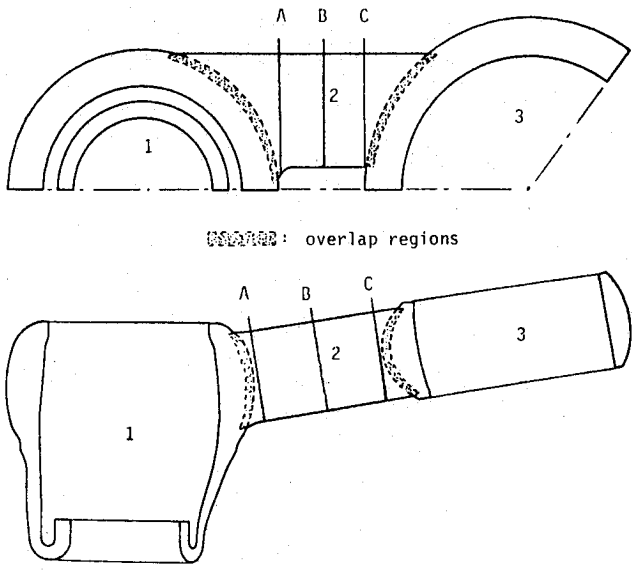

Fig. 6 Multiple computational zones.

where $|\omega|$ is the absolute value of the three-dimensional vorticities. In the inner sublayer, the Van Driest damping function is applied to make corrections for the viscous effects.

Boundary Conditions

For the current HGM configuration, the vertical plane through the center of the fuel bowl and the main injector is taken to be a plane of symmetry; hence, only half of the HGM is used in the formulation of the problem. Symmetric boundary conditions are applied at this plane. It is known in the literature that specification of a total pressure for the inflow and a static pressure for the outflow is a very good physical boundary condition for subsonic internal flow simulations. However, for the current complex flow in the HGM, the static pressure is not known a priori at the outlet. Therefore, the following boundary conditions are proposed. On the solid surfaces, no-slip boundary conditions and zero normal pressure gradients are specified. A static pressure and a velocity profile are given at the inlet of the TAD. As explained earlier, uniform radial outflow may be used to approximate the flow entering into the main injector region. Thus, a uniform radial outflow satisfying conservation of mass is specified at the outlet surface. The velocity components other than the radial one and the pressure at this plane are obtained by second-order extrapolations. At the radial end plane of the 70% racetrack, it is assumed that there is no outflow in the circumferential direction.

Zonal Boundary Values and Overlapped Interior Regions

In utilizing the multiple zones, boundary conditions are needed at the interfaces. The pressure and the velocities Q are updated at each iteration. Let $n+\frac{1}{2}$ denote the state of conditions to be used to advance the computation to $n+1$. The values of $Q^{n+\frac{1}{2}}$ for zone m at the exit plane are obtained from the values of the corresponding plane of zone $m+1$ at n, i.e.,

$$\left[Q_{\text{BC}}^{n+\frac{1}{2}}\right]_{\text{zone } m} = \left[Q_{\text{interior}}^{n}\right]_{\text{zone } m+1} \tag{6}$$

and values of $Q^{n+\frac{1}{2}}$ for zone $m+1$ at the zonal interfaces are taken from the latest computed result of zone m as

$$\left[Q_{\text{BC}}^{n+\frac{1}{2}}\right]_{\text{zone } m+1} = \left[Q_{\text{interior}}^{n+1}\right]_{\text{zone } m} \tag{7}$$

To provide a smooth continuation of solution, the latest information, not only at the boundary but also including the interior of this mutually occupied region, must be properly transmitted to the next zone. The current approach is to take an average of the two values computed in the neighboring zone, i.e.,

$$\left[Q^{n+\frac{1}{2}}\right] = \tfrac{1}{2}\left(\left[Q^{n}\right]_{\text{zone } m+1} + \left[Q^{n+1}\right]_{\text{zone } m}\right) \tag{8}$$

Computed Results

Steady-state laminar and turbulent flow solutions for the HGM configuration including the fuel side TAD, the annular fuel bowl, the elliptical transfer duct, and 70% racetrack of the main injector are obtained, respectively. The Reynolds number, based on the width of the TAD entrance and the inlet velocity, is 10^3 for the laminar flow and 1.9×10^6 for the turbulent flow. The same boundary conditions are used in both flow simulations.

Figure 7 shows the velocity vectors of the turbulent flow solution at two cross-sectional planes. Laminar flow solution reveals similar flow characters at these planes and, hence, is not shown here. There is no streamwise flow separation along the transfer duct shown in Fig. 7. In contrast to the three-duct design, the current two-duct configuration effectively eliminates the large separation bubble formed just downstream of the entrance to the transfer ducts.[7] Figure 8 shows the velocity profiles for both laminar and turbulent flows at three TAD cross-sectional planes. The figure shows that a large separated

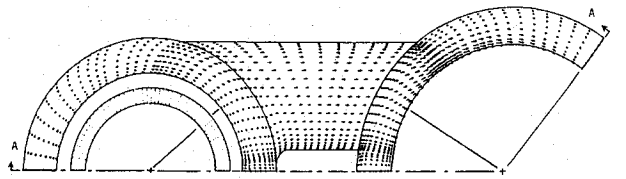

a) Horizontal view: cross-section B-B

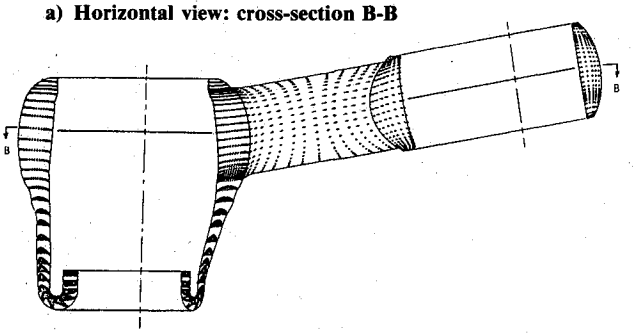

b) Vertical view: cross-section A-A

Fig. 7 Computed velocity vectors.

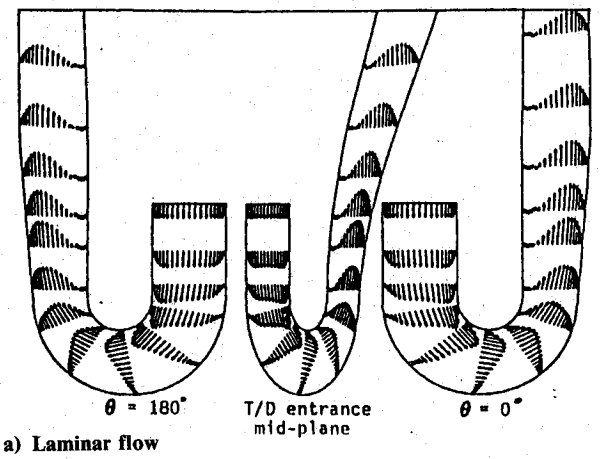

a) Laminar flow

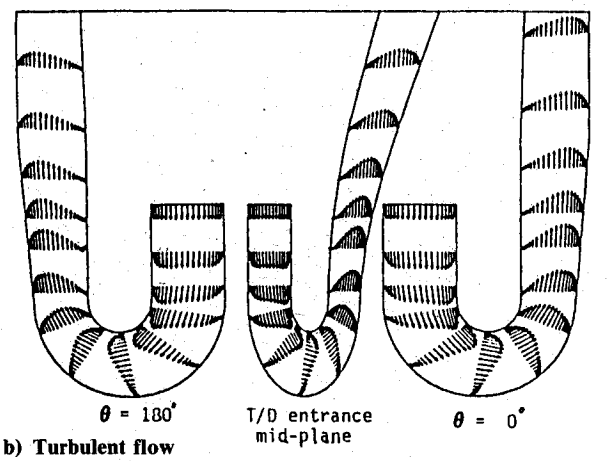

b) Turbulent flow

Fig. 8 TAD cross-sectional velocities.

flow region exists in the TAD for the case of laminar flow, whereas only a small separation is indicated in the corresponding location for the turbulent case. In turbulent boundary-layer flows, the fiuid particle near the wall, except in the very thin viscous sublayer, has much higher kinetic energy than the corresponding laminar flows. Consequently, the turbulent flow is more able to sustain the adverse pressure gradient in the sharp turn, resulting in a smaller separation bubble. In the laminar case, the less full velocity profile together with the larger separation zone creates a larger blockage effect. The resulting flow, therefore, must have a higher upward velocity to satisfy conservation of mass.

Figure 9 illustrates the swirling flow patterns at the three cross-sectional planes indicated in Fig. 6 along the transfer duct. The intensity of the swirling flow depends on the upward velocity of the fluid coming from below the transfer duct. Since laminar flow has a larger blockage effect, resulting in a higher upward velocity, the magnitude of the swirling flow is expected to be higher than the turbulent case. The computed maximum magnitude of the swirling velocity near the duct entrance for the laminar flow is 0.44 relative to the inlet velocity; it is 0.33 for the turbulent case. The swirling flows are gradually dissipated along the duct. The secondary flow patterns are different from those obtained by Chang et al.[7-9] The different flow phenomena are due to the different downstream boundary condition and the different geometry used in the present calculation.

Figure 10 shows mass-weighted average total pressure distributions along the centerline of the TAD, the fuel bowl, the transfer duct, and the racetrack for both flows. From this figure, it is clear that most of the pressure loss occurs in the TAD where flow experiences a 180-deg turn. Significant losses are also observed in the fuel bowl due to flow separations, the

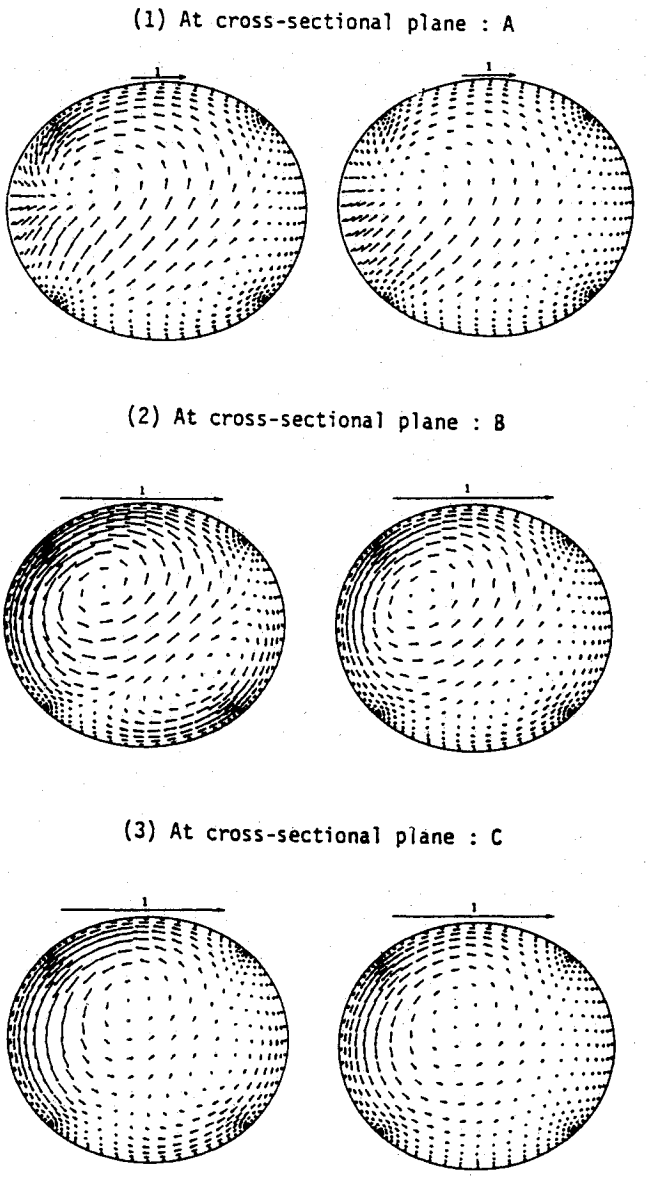

a) Laminar flow b) Turbulent flow

Fig. 9 Secondary velocities in transfer duct.

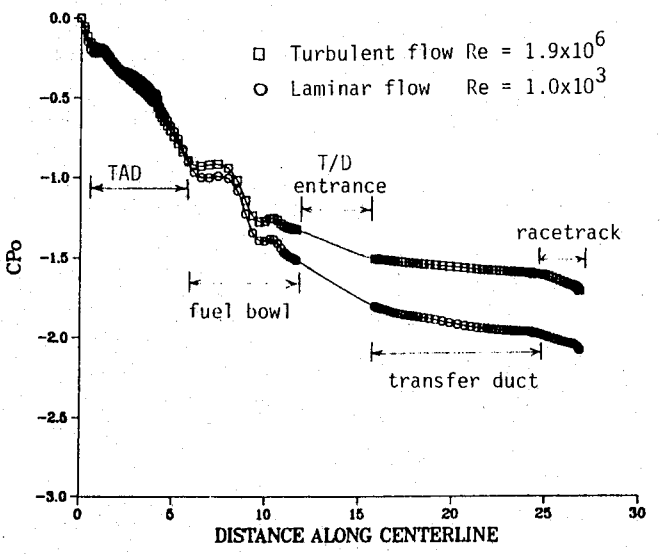

Fig. 10 Coefficient of total pressure distribution.

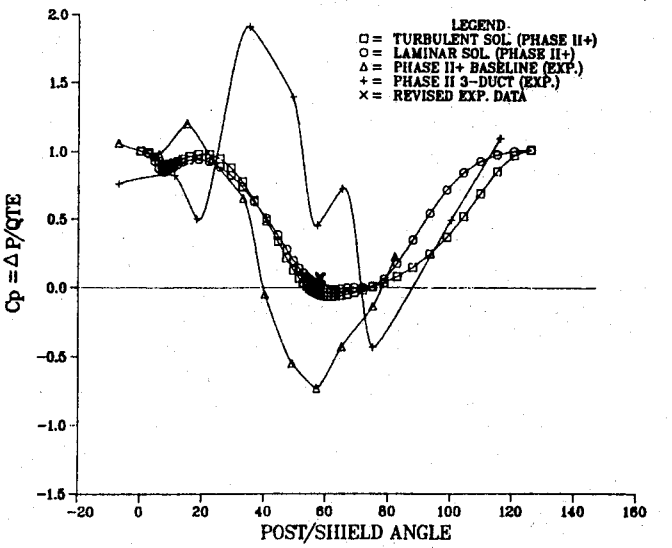

Fig. 12 Shield pressure loading.

transfer duct entrance region because of the strong swirling flow, and the racetrack outlet region caused by the flow impingement on the shield and post arrangement. As expected, the turbulent flow yields a lower total pressure loss. Figure 11 illustrates the computed and the measured transverse pressure coefficients at the fuel bowl outer surface immediately downstream of the 180-deg bend. Overall, the agreement with the experiment[10] is satisfactory. The small difference shown is due to the fact that at the inlet the pressure is assumed to be uniform in the calculation, whereas it is not uniform in the experiment. Furthermore, there are struts fixed inside the fuel bowl in the test environment and no struts are assumed in the current calculation. The calculation results, as confirmed by the experiment, clearly demonstrate a great reduction in the transverse pressure gradient for the two-duct configuration over the three-duct ones. Reducing the transverse pressure gradient can greatly enhance the engine performance.

It is interesting to calculate the pressure loading across the shield and post arrangement for the structure design purpose. A simple model is proposed to derive from the current solution to obtain the loading without solving the complex flowfield behind the shield. Recall that at the outlet surface the radial outflow was assumed to be uniform. In reality, the flow has to pass through the small gaps and holes to enter into the LOX post region (see Fig. 3). By assuming that the total pressure loss across the gaps is negligible and the static pressure at the back of the shield is equal to the one at the gap exit, the pressure loading on the shield can then be easily obtained from conservation of mass and energy. In mathematical form, the conservation of mass yields $V_e = V_i \times A_i/A_e$, and the conservation of energy gives $P_i + 0.5 \times (u_i^2 + v_i^2 + w_i^2) = P_e + 0.5 \times V_e^2$, where V_i is the specified uniform radial outflow, V_e the estimated velocity entering the gaps, A_i and A_e the corresponding flow areas ahead of the shield surface and at the gap exit, u_i, v_i, w_i the Cartesian velocity components at the shield surface, and P_i and P_e the pressure at the shield surface and at the gap exit, respectively. The pressure loading on the shield can be obtained from the difference between P_i and P_e. Figure 12 compares the result of the calculation and the experimental data.[10] The data were obtained by the measurements of shield pitot probes. The probes were intruded into the flowfield. Analogous to a cylinder in crossflow, the intrusion of the probes resulted in providing lower than true pressure measurements. In the neighborhood of the 60-deg region, the test data is not yet conclusive. Comparing with a revised data point shown at the 60-deg location, the overall computed result is encouraging.

Concluding Remarks

This paper presents a further development of the INS3D code and its application to the real-world complex problems.

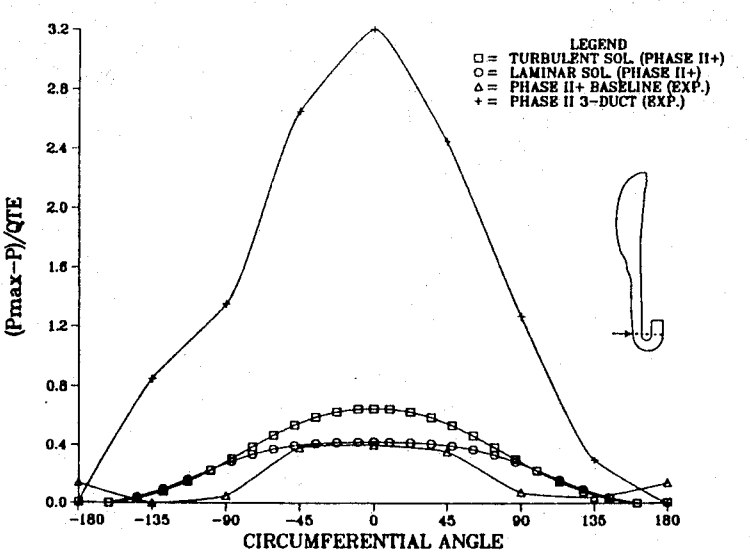

Fig. 11 Coefficient of transverse pressure after 180-deg bend.

Three-dimensional incompressible laminar and turbulent flows in the fuel side hot gas manifold of the Space Shuttle main engine have been computed. Computed results are in good qualitative agreement with available experimental data. The present work has provided an in-depth understanding of the dynamics of the flow in the HGM configuration. The results were obtained through assumptions of a symmetry plane and a no outflow boundary at 70% racetrack location. It should be noted that the turbopump would introduce a swirling velocity at the inflow boundary of the annular turnaround duct, which is precluded by the symmetry boundary. This might change the nature of separation in the duct. Also, there is fluid mixing of fuel and oxidizer in the racetrack and a nonradial interface, which are precluded by the current racetrack outflow boundary conditions. For a quantitative comparison, exact flow environments, for instance, the struts sitting inside the fuel bowl as well as the informations at inlet and outlet boundaries, should be implemented into the simulation.

Acknowledgments

This work was sponsored by NASA Marshall Space Flight Center. Computations were carried out at NASA Ames Research Center. The authors are grateful to G. Ratekin of Rocketdyne and P. Kutler of NASA Ames Research Center for their support and encouragement during the course of this study.

References

[1]Beam, R. M., and Warming, R. F., "An Implicit Finite-Difference Algorithm for Hyperbolic Systems in Conservation-Law Form," *Journal of Computational Physics,* Vol. 22, Sept. 1976, pp. 87–110.

[2]Briley, W. R., and McDonald H., "Solution of the Multidimensional Compressible Navier-Stokes Equations by a Generalized Implicit Method," *Journal of Computational Physics,* Vol. 24, Aug. 1977, pp. 372–397.

[3]Chorin, A. J., "A Numerical Method for Solving Incompressible Viscous Flow Problems," *Journal of Computational Physics,* Vol. 2, No. 12, 1967, pp. 12–16.

[4]Steger, J. L., and Kutler, P., "Implicit Finite-Difference Procedures for the Computation of Vortex Wakes," *AIAA Journal,* Vol. 15, No. 4, 1977, pp. 581–590.

[5]Chang, J. L. C., and Kwak, D., "On the Method of Pseudo-Compressibility for Numerically Solving Incompressible Flows," AIAA Paper 84-0252, Jan. 1984.

[6]Kwak, D., Chang, J. L. C., Shanks, S. P., and Chakravarthy, S. R., "A Three-Dimensional Incompressible Navier-Stokes Flow Solver Using Primitive Variables," *AIAA Journal,* Vol. 24, No. 3, 1986, pp. 390–396.

[7]Chang, J. L. C., Kwak, D., Dao, S. C., and Rosen, R., "A Three-Dimensional Incompressible Flow Simulation Method and Its Application to the Space Shuttle Main Engine, Part 1—Laminar Flow," AIAA Paper 85-0175, Jan. 1985.

[8]Chang, J. L. C., Kwak, D., Dao, S. C., and Rosen, R., "A Three-Dimensional Incompressible Flow Simulation Method and Its Application to the Space Shuttle Main Engine, Part 2—Turbulent Flow," AIAA Paper 85-1670, July, 1985.

[9]Chang, J. L. C., Yang, R.-J., and Kwak, D., "A Full Navier-Stokes Simulation of Complex Internal Flows," *Proceedings of 10th International Conference on Numerical Method in Fluid Dynamics,* Lecture Notes in Physics, Springer-Verlag, New York, 1986, pp. 154–160.

[10]O'Connor, G. M., "SSME Phase II+ Hot Gas Manifold Airflow Test Evaluation—Interim Report," Rockwell International, Rocketdyne Rept. RSS-8714, Canoga Park, CA, March 1986.

Ernest V. Zoby
Associate Editor